ACS NANO

www.acsnano.org

ARTICLE

The Conductance Isotope Effect in Oligophenylene Imine Molecular Wires Depends on the Number and Spacing of ^{13}C-Labeled Phenylene Rings

Abraham Colin-Molina, Tahereh Nematiaram, Andy Man Hong Cheung, Alessandro Troisi, and C. Daniel Frisbie*

Cite This: *ACS Nano* 2024, 18, 7444−7454

Read Online

ACCESS | Metrics & More | Article Recommendations | Supporting Information

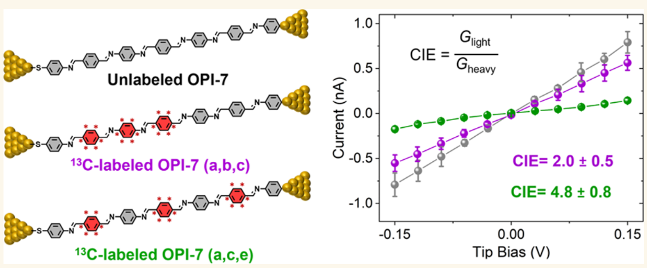

ABSTRACT: **We report a strong and structurally sensitive ^{13}C intramolecular conductance isotope effect (CIE) for oligophenyleneimine (OPI) molecular wires connected to Au electrodes. Wires were built from Au surfaces beginning with the formation of 4-aminothiophenol self-assembled monolayers (SAMs) followed by subsequent condensation reactions with ^{13}C-labeled terephthalaldehyde and phenylenediamine; in these monomers the phenylene rings were either completely ^{13}C-labeled or the naturally abundant ^{12}C isotopologues. Alternatively, perdeuterated versions of terephthalaldehyde and phenylenediamine were employed to make ^{2}H(D)-labeled OPI wires. For ^{13}C-isotopologues of short OPI wires (<4 nm) in length where the charge transport mechanism is tunneling, there was no measurable effect, i.e., ^{13}C CIE ≈ 1, where CIE is defined as the ratio of labeled and unlabeled wire resistances, i.e., CIE = R_{heavy}/R_{light}. However, for long OPI wires >4 nm, in which the transport mechanism is polaron hopping, a strong ^{13}C CIE = 4−5 was observed. A much weaker inverse CIE < 1 was evident for the longest D-labeled wires. Importantly, the magnitude of the ^{13}C CIE was sensitive to the number and spacing of ^{13}C-labeled rings, i.e., the CIE was structurally sensitive. The structural sensitivity is intriguing because it may be employed to understand polaron hopping mechanisms and charge localization/delocalization in molecular wires. A preliminary theoretical analysis explored several possible explanations for the CIE, but so far a fully satisfactory explanation has not been identified. Nevertheless, the latest results unambiguously demonstrate structural sensitivity of the heavy atom CIE, offering directions for further utilization of this interesting effect.**

KEYWORDS: *molecular wires, conductance isotope effect (CIE), polaron, charge transport, hopping*

INTRODUCTION

Kinetic isotope effects (KIEs) are extensively employed to understand reaction mechanisms, and it would be difficult to overstate their importance to the development of modern chemistry.[1−3] ^{2}H(D), ^{13}C, and ^{15}N isotope substitutions are all relatively common, with D-substitution constituting the bulk of KIE studies because the effect of deuteration on C−H bond breaking or formation rate constants k is large (e.g., $k_H/k_D \approx$ 1−10) and deuteration of organic molecules is relatively straightforward and inexpensive.[4] ^{13}C- and ^{15}N-Labeling are more expensive, and the impact of these heavy atom isotopes on bond breaking or formation rate constants is substantially smaller, typically a few percent or less. This is well understood, as the zero-point energies E_{ZPE} of C−C bonds, for example, which influence many reaction barriers, are not strongly impacted by the 8% mass difference between ^{12}C and ^{13}C ($E_{ZPE,12C}/E_{ZPE,13C} \propto \sqrt{M_{13C}/M_{12C}}$ = 1.04).[5,6] Nevertheless, both ^{13}C and ^{15}N labeling are commonly used to examine the mechanisms of many types of reactions.[7−12]

In this context, our initial discovery of an enormous ^{13}C and ^{15}N isotope effect on the intramolecular electrical conductance of pi-conjugated oligomers was surprising.[13] These experi-

Received: November 14, 2023
Revised: February 11, 2024
Accepted: February 15, 2024
Published: February 27, 2024

https://doi.org/10.1021/acsnano.3c11327
ACS Nano 2024, 18, 7444−7454

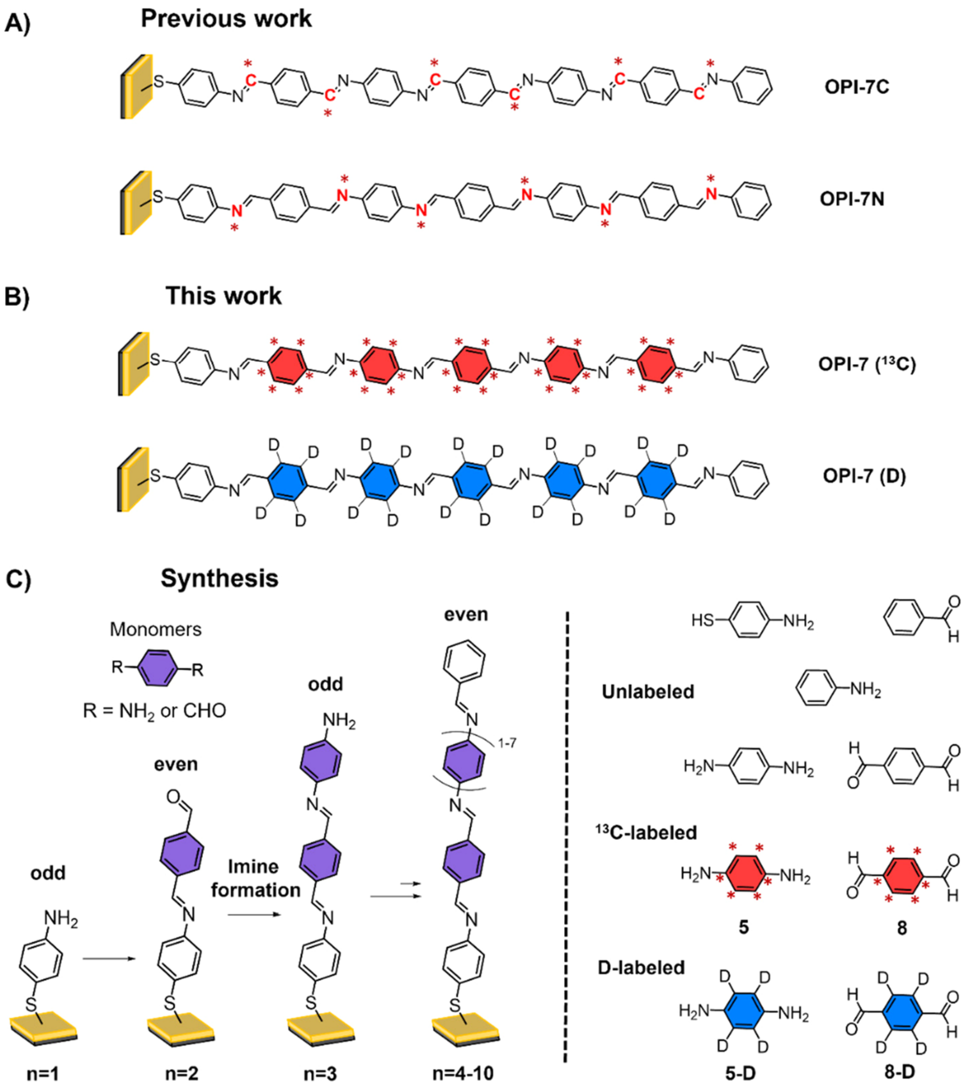

Figure 1. Chemical structures of example oligophenyleneimine wires with seven phenylene rings (OPI-7) where (A) the imine groups are labeled with ^{13}C or ^{15}N atoms (*) and (B) the aromatic rings are labeled with ^{13}C (*) or D atoms. (C) Stepwise synthesis of OPI wires and chemical structure of monomers used in the synthesis. Purple colored rings indicate the ^{13}C or D-labeled units in the wires, and *n* is the number of rings in the oligomer.

ments employed oligophenyleneimine (OPI) wires ranging in length from 1 to 7 nm that were built from Au surfaces using a previously reported synthesis[14] based on sequential condensation reactions of 1,4-benzenediamine and terephthalaldehyde, Figure 1. ^{13}C- and ^{15}N-Labeling of the imine −C═N− linkages was achieved using 1,4-benzenediamine-$^{15}N_2$ and terephthalaldehyde-$^{13}C_2$ as reagents. The low-bias resistances R_{heavy} and R_{light} of the labeled and unlabeled isotopologues, connected at either end to Au electrodes, were measured using conducting probe atomic force microscopy (CP-AFM) in which an Au-coated AFM tip makes the second contact.[15−17] We observed that for short OPI wires less than 4 nm in length, where the electrical conductance mechanism is off-resonant tunneling,[18] there was no conductance isotope effect (CIE), i.e., CIE = $R_{heavy}/R_{light} \approx 1$. However, for longer OPI wires (>4 nm), where it is well established that the transport mechanism is charge hopping,[19] the $^{13}C/^{15}N$ CIE was of order 10, a very large value. Deuteration of the imine proton produced no measurable CIE.

Here, our goal is to expand understanding of the heavy atom CIE in OPI wires by exploring its sensitivity to structurally selective labeling. In particular, we have ^{13}C-labeled the phenylene rings, Figure 1B, in contrast to labeling the imine bonds, which we reported before,[13] Figure 1A. We observe a very strong ^{13}C CIE = 4−5 associated with the labeled rings. We have also perdeuterated the rings as shown. The effects of deuteration are small but are perhaps not negligible compared to the uncertainty in the measurements. Interestingly, the D-CIE appears to be <1 for the longest wires, i.e., it is an "inverted" CIE. We have also systematically varied the number and spacing of the ^{13}C-labeled rings in the OPI oligomers and these changes greatly impact the measured CIE. That is, we find that the CIE is structurally sensitive. We propose that this discovery will facilitate understanding of polaron hopping mechanisms and charge localization/delocalization phenomena in pi-conjugated oligomers with a high degree of structural precision. Full utilization of this effect will require theoretical understanding, and we describe our attempts so far to explain the CIEs. To date, full theoretical understanding of the ^{13}C−CIE is not in hand. We have examined a number of potential explanations, and so far, none of them appear satisfactory, as will be described toward the end of this article.

https://doi.org/10.1021/acsnano.3c11327
ACS Nano 2024, 18, 7444−7454

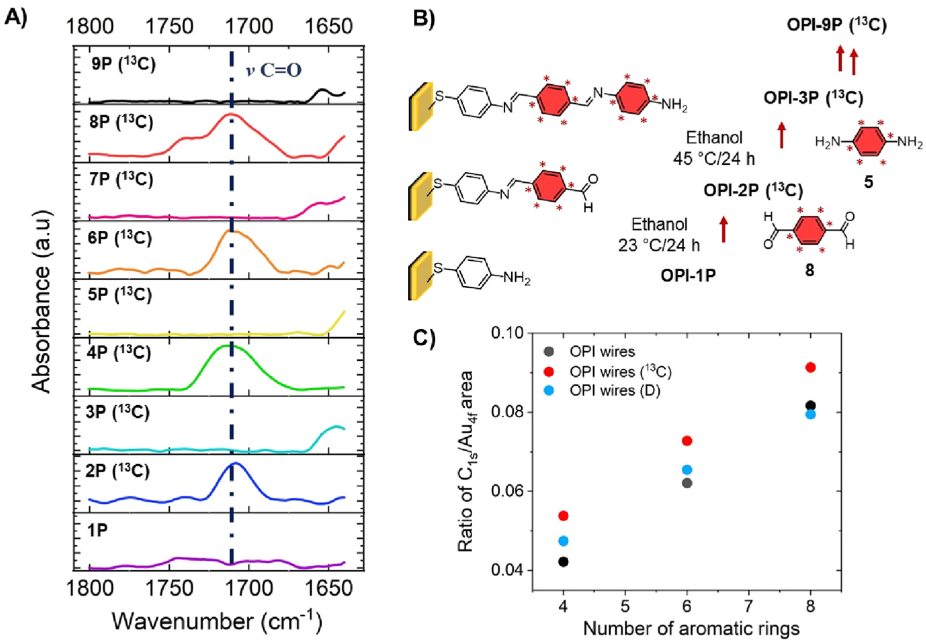

Figure 2. Stepwise characterization of ^{13}C-labeled OPI wires. (A) RAIRS spectra for OPI-*n*P (*n* = 1−9) where P denotes precursor indicating that wires are not capped with terminal phenyl rings. (B) Scheme of the imine click reaction using monomers 5 and 8 to grow the target molecular wires. (C) Plot of the ratio of C_{1s}/Au_{4f} peak areas (285.0 vs 84.0 eV) from XPS analyses showing similar carbon content for the three isotopologues with the same number of aromatic rings and indicating comparable surface coverage.

Nevertheless, our experimental findings significantly expand our initial report.[13] We provide evidence that labeling the phenylene rings results in a ^{13}C CIE that is comparable to but somewhat smaller than labeling the imine linkages. Additionally, we show that the ^{13}C CIE is structurally sensitive. This finding is critical, as structural sensitivity potentially changes the CIE from a curious observation to an analytical tool. We propose that with further development, the heavy atom CIE could advance the understanding of polaron transport in molecular systems in a manner similar to the utility of the KIE for understanding reaction mechanisms in chemistry.

RESULTS AND DISCUSSION

Growth and Characterization of Oligophenyleneimine (OPI) Wires. Oligophenyleneimine (**OPI*n***) wires with different molecular lengths (1−7 nm) corresponding to the number of aromatic rings *n* in the structure (*n* = 1−10) were prepared by sequential imine "click" reactions using the monomers terephthalaldehyde or 1,4-diaminobenzene alternatively (Figure 1C). This synthetic strategy has excellent yield and allows us to (1) precisely control the molecular length and (2) insert desired monomer units at specific locations in the molecular structure.[20−23] To build the OPI isotopologues, we first performed the synthesis of the ^{13}C- and D-labeled monomers (Figure 1C), according to the procedures detailed in "Materials and Methods" section and Scheme S1 in the Supporting Information. For the monomer synthesis, we used commercially available aniline-$^{13}C_6$, benzene-$^{13}C_6$, or their fully deuterated analogues as starting materials, and target compounds **5**, **5-D**, **8**, and **8-D** were isolated in good yields. All compounds were characterized by NMR in solution (Figures S21−S34), and their purity was confirmed to be higher than 99% by this technique.

With monomers in hand, synthesis of the OPI wires was carried out as described in Figures S1−S3. To confirm the success of the imine condensation reactions at every step in the OPI wire growth, reflection−absorption infrared spectroscopy (RAIRS), and high-resolution X-ray photoelectron spectroscopy (XPS) analyses were performed. In the RAIRS spectra we followed the peak at ∼1712 cm^{-1} associated with the C═O stretch from the terminal aldehyde group in *n* = even OPI wires and the full disappearance of this peak in the next *n* = odd OPI wire, Figure 2A and Figures S4 and S5.[14,22,23] Note that achieving complete reaction of aldehyde-terminated wires with the benzene diamine (*n* = even to *n* = odd), and the corresponding full disappearance of the surface C═O peak, required an elevated reaction temperature. Incubation at 40 °C for 24 h was sufficient for both the unlabeled wire and perdeuterated wire synthesis, but for the ^{13}C-labeled wire synthesis, we found complete reaction of all surface aldehyde required 45 °C for 24 h. There seemed to be a heavy atom effect on the reaction kinetics for *n* = even to *n* = odd additions; incubation at room temperature (23 °C) was sufficient in all cases for *n* = odd to *n* = even additions.

Comparison of the RAIRS spectra for all OPI wires in the range of 1850−1350 cm^{-1} in Figure S6 shows changes in the molecular vibrational modes upon labeling: (1) The peaks at 1712 and 1618 cm^{-1} assigned to the carbonyl (C═O) and imine (R-CH═N-R) stretching, respectively, remain essentially at the same location in all cases because the ^{12}C/^{13}C exchange in the rings does not affect the imine connectivity. (2) In the aromatic C═C stretching region (1625−1400 cm^{-1}), a peak at ∼1580 cm^{-1} associated with extended conjugation of rings was observed in all samples consistent with wire growth. (3) Four main peaks (∼1516, 1481, 1437, and 1409 cm^{-1}) were found in the same region for OPI and D-labeled OPI wires while only one intense peak near 1480 cm^{-1} was observed for ^{13}C-labeled OPI wires, demonstrating that the skeletal vibrations are affected by the mass change due to ^{13}C-labeling.

To complement the RAIRS characterization, we carried out XPS measurements for unlabeled and labeled **OPI-4P**, **OPI-**

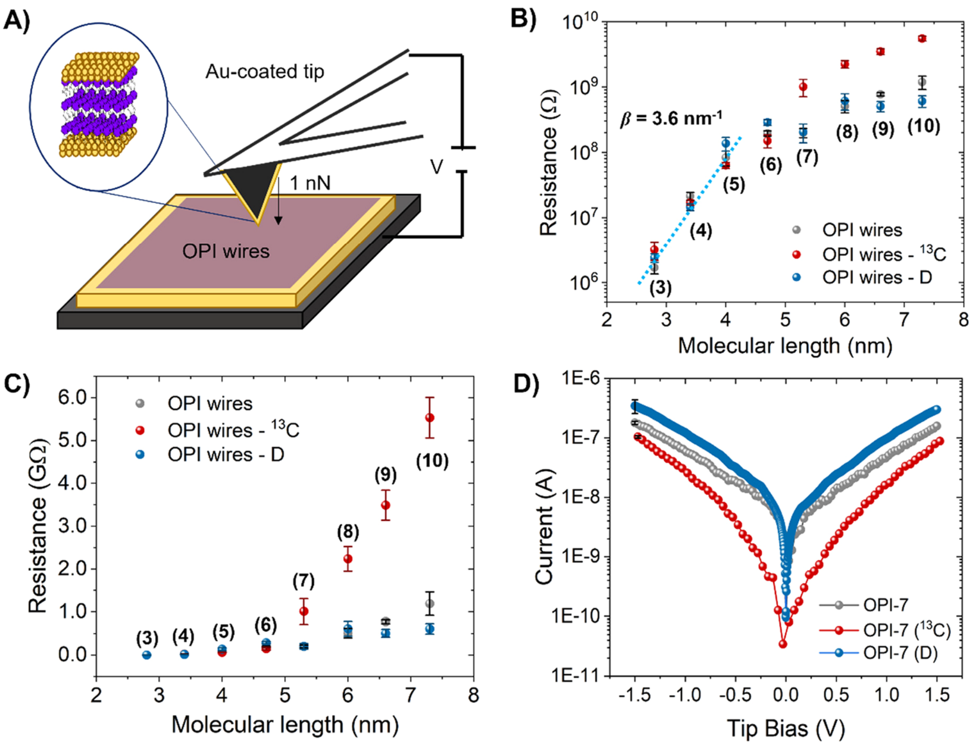

Figure 3. (A) Representation of a molecular junction formed by using conducting probe atomic force microscopy (CP-AFM). (B) and (C) Semilog and linear plots of low bias resistance versus molecular length for unlabeled and labeled OPI wires. Each data point is the average of resistances extracted from 800 *I*−*V* traces within ±0.15 V. Error bars represent standard error. D) Semilog plot of the average current from 250 *I*−*V* traces within ±1.5 V for the three isotopologues of OPI-7. Error bars represent standard errors.

6P, and **OPI-8P** wires, where P denotes "precursor" wires that have not been terminated with aniline or benzaldehyde. The XPS data were analyzed in detail. The fitting of the C_{1s} peak showed that the OPI wires consist of aromatic C atoms with a peak at 285.0 eV and also imine (C═N) C atoms, which exhibit a minor peak at 286.1 eV. The N_{1s} spectral region exhibits one peak at 399.2 eV confirming the presence of C═N bonds in the molecules (Figures S7−S9).[24] The fitting of the XPS spectra for the three isotopologues (normal, D-labeled, and ^{13}C labeled) resulted in excellent fits (R^2 values higher than 0.997 for C_{1s}), which allowed us to calculate the peak areas for all peaks mentioned above (see Tables S1−S3). A plot of the ratio of C_{1s}/Au_{4f} peak areas (using peaks at 285.0 and 84.0 eV, respectively) as a function of the number of monomers (Figure 2C) showed that the C content was similar for molecular wires with the same molecular length. As expected, there is a clear increase of the ratioed C_{1s}/Au_{4f} peak areas with the addition of aromatic rings. Similar results were found for the N content, as evident in Figure S10. We conclude that the stepwise surface synthesis produced the natural and ^{13}C- and D-labeled **OPI-*n*** (*n* = 3−10) isotopologues with comparable surface coverages (e.g., differences within 15% for OPI-8 isotopologues). We then performed electrical characterization for all 24 types of molecular wires.

Electrical Characterization of OPI Wires. To measure the conductance *G* and resistance *R* of the OPI wires, we employed the CP-AFM platform under a controlled atmosphere (Ar). Au-coated tips were brought into soft contact (∼1 nN) with the OPI wires molecules, Figure 3A, making *in situ* molecular junctions with a contact area of about 25 nm^2.[25−27] For these experiments, we employed a Keithley 236 source measure unit operated in "DC mode" to apply voltages to the tip relative to the grounded substrate. For each type of molecular wire (distinguished by length and isotopic labeling pattern), we measured approximately 800 *I*−*V* curves within ±0.15 V in several locations on several samples at room temperature; the averaged *I*−*V* traces are shown in Figures S11−S13, and they are all linear in this voltage range. The low bias conductance *G* of every molecular wire was estimated from the slope, and the resistance *R* was calculated as the inverse of the conductance ($R = 1/G$). The semilog plot of low bias resistance versus molecular length shown in Figure 3B reveals an exponential increase in the resistance as a function of the molecular length for **OPI-3−5**, and most importantly, it shows similar resistance values for all three isotopologues of these short wires with lengths of <4 nm. There is no apparent CIE, consistent with our previous results on short OPI wires with labeled imine bonds.[13]

For short wires, the transport mechanism is off-resonant tunneling, and resistance *R* scales exponentially with molecular length *L* according to eq 1:[28−30]

$$R = R_0 \exp(\beta L) \tag{1}$$

where R_0 is the resistance prefactor and β is the tunneling attenuation coefficient. From the linear fit of the semilog wire resistance plot (blue dotted line in Figure 3B), we calculated β = 3.6 nm^{-1} which is within the range of reported values for conjugated systems.[31−34]

As the wire length increases beyond **OPI-5** to **OPI-6** and up to **OPI-10**, there is a clear decrease in the sensitivity of resistance to length, Figure 3B,C. The functional length dependence of resistance changes from exponential to roughly linear. As we have shown in previous work, this change

https://doi.org/10.1021/acsnano.3c11327
ACS Nano 2024, 18, 7444−7454

corresponds to a crossover in charge transport mechanism from tunneling to hopping.[14,18,19,35] Most importantly, inspection of Figure 3B,C shows that there is a clear CIE for the ^{13}C labeled wires in the hopping regime. We take CIE = G_{light}/G_{heavy} = R_{heavy}/R_{light}. The effect is significant: there is about a factor of 5 increase in the low bias resistance for ^{13}C-labeled wires **OPI-7−10** compared to the unlabeled isotopologues, as summarized in Table 1. In a control experiment, we checked whether small differences (45 vs 40 °C) in the diamine addition step for ^{13}C-labeled and unlabeled OPI wires could be responsible for the large differences in resistance. We found no effect of these small growth temperature differences on wire resistance (Supporting Information). Interestingly, the situation is more complicated for the D-labeled isotopologues. For D-labeled **OPI-6** and **OPI-7**, there is no discernible CIE. However, for **OPI-8−10**, it seems that there is a small inverse CIE < 1, i.e., the resistances of the longest D-labeled molecules appear to be somewhat lower, by a factor of 0.7, than the unlabeled molecules (Table 1). Inverse KIEs are also well-known in organic chemistry and have been observed recently for charge transfer and oxygen reduction reactions.[36−40] However, we caution here that this small effect is only slightly greater than the molecular coverage differences we might expect for different samples. Even though the data in Figure 3B,C reflect hundreds of measurements on multiple samples, we cannot be absolutely certain from the low bias data that the apparent inverse CIE for the D-labeled wires is real. Further repetition of these measurements is warranted.

Table 1. Summary of the Low-Bias Conductance Isotope Effect (CIE) for ^{13}C and D-Labeled OPI Wires[a]

OPI-*n* wire	CIE ^{13}C-labeled	CIE D-labeled
6	0.8 ± 0.2	1.5 ± 0.2
7	5.0 ± 1.7	1.1 ± 0.4
8	4.7 ± 1.0	1.2 ± 0.4
9	4.5 ± 0.5	0.7 ± 0.1
10	4.9 ± 1.1	0.6 ± 0.2

[a]CIE = R_{heavy}/R_{light} where R_{heavy} is the low bias (±0.15 V) resistance of the heavy atom isotopologue and R_{light} is the low bias resistance of the natural abundance isotopologue. Uncertainties are standard errors on the mean.

We also measured the full $I-V$ characteristics over ±1.5 V for all unlabeled and ^{13}C/D-labeled wires with n >7 (Figures S14−S17). The overlay of averaged traces (250 $I-V$ curves in several locations of different samples) for the three isotopologues of **OPI-7** is shown in Figure 3D on a semilog scale. This plot demonstrates that the fully ^{13}C-labeled wire has a significantly lower current than that of its unlabeled analogue across the whole bias window. Inspection of the traces also suggests that the *differential* CIE has voltage dependence, i.e., the ratio of differential resistances (differential CIE = dR_{heavy}/dR_{light} where $dR = dV/dI$) is not constant. Further measurements of the voltage dependence of the differential CIE are the subject of ongoing work. We note that the Figure 3D data also indicate that there is a measurable and bias-dependent inverse CIE < 1 for the deuterated wires compared to the unlabeled wires at all biases, and a fuller investigation of this effect is also the subject of future work. All of the data in Figure 3D are broadly consistent with the low bias results in Figure 3C. Again, for small isotope effects like the ones observed for the D-labeled isotopologues at low bias, particular attention must be paid to wire surface coverage,[22] such that small differences in wire coverage, leading to small differences in resistance for the normal and fully labeled isotopologues are not anomalously attributed to an isotope effect.

In summary, for this part, we observe a clear ^{13}C heavy atom CIE when the phenylene rings in the OPI wires are labeled. The size of the effect is comparable to, though somewhat smaller than, what we observed previously for ^{13}C labeling of the imine carbon atoms.[13] The complete absence of a CIE for short molecules of <4 nm in length, and the prevalence of a strong CIE for molecules above this length, is also further support for a change in conduction mechanism as a function of wire length. That is, our labeling experiment is consistent with a crossover from tunneling to hopping conduction as length increases as has been observed in different wire backbones.[14,41−43]

Before turning to theoretical considerations, we provide one additional piece of information. We have measured the temperature dependence of the low bias resistance for ^{13}C-labeled **OPI-7** wires and the unlabeled version (Figure 4). We see that the resistance is activated, with lower temperatures producing higher resistance, as expected for hopping transport, and in line with our previous investigations.[14,19,35,44] The activation energies for ^{13}C **OPI-7** and unlabeled **OPI-7** are similar, and both are ∼400 meV (∼9 kcal/mol). As shown in Figure 4 the actual values for ^{13}C **OPI-7** and unlabeled **OPI-7** are 461 and 355 meV, respectively. We caution against overinterpretation of these values as the examined temperature range is quite small (50 K) due to limitations of our experimental setup. More extensive measurements down to 10 K are planned and will be reported in future work. However, the measured activation energies are in line with our previous measurements on unlabeled OPI wires, and they are consistent with hopping transition states calculated earlier by Cramer and Gagliardi.[28,45] These earlier quantum chemical calculations noted that the OPI wires are decidedly not planar with significant ring torsions along the backbone. The calculations also suggested that the transition state involves ring motion to produce locally planar (and more pi-conjugated) segments, which would facilitate charge hopping. The activation energies of ∼400 meV are consistent with this picture.

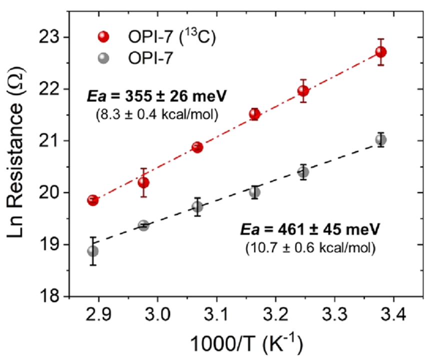

Figure 4. Arrhenius plot for OPI-7 and ^{13}C-labeled OPI-7. The activation energies were obtained from the slope of linear fits. Each point corresponds to the average of the low bias resistance in several locations of different samples. Error bars represent standard errors on the mean.

https://doi.org/10.1021/acsnano.3c11327
ACS Nano 2024, 18, 7444−7454

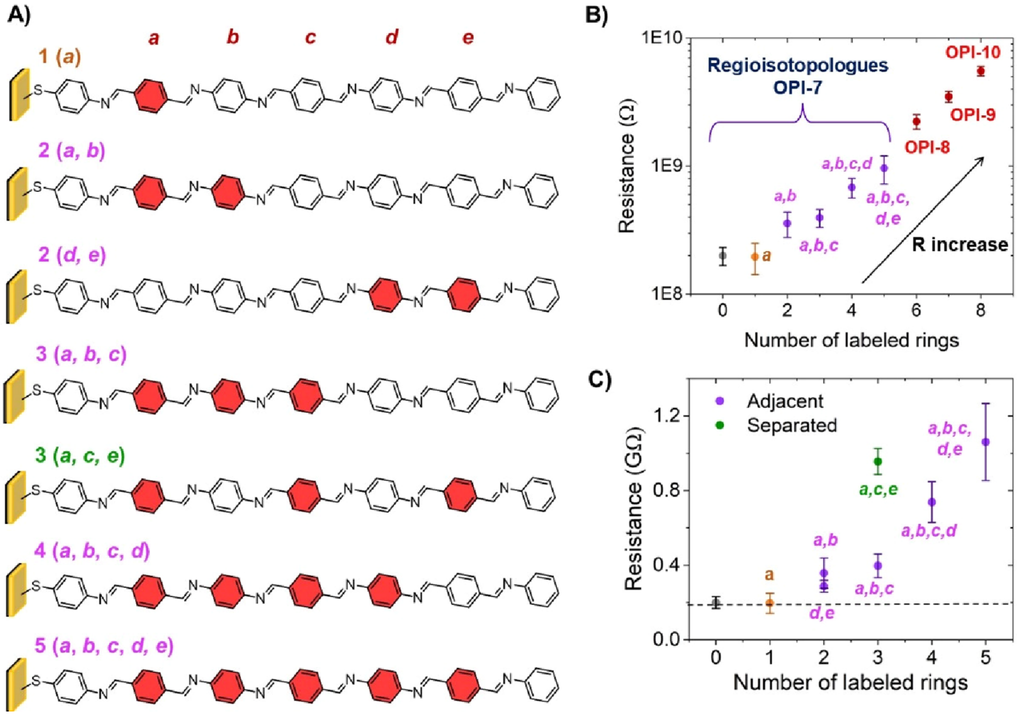

Figure 5. (A) Molecular structures of OPI-7 isotopologues with adjacent (e.g., 3a,b,c) and separated (e.g., 3a,c,e) ^{13}C-labeled rings. (B) Semilog plot of resistance vs number of adjacent labeled rings for OPI wires with $n \geq 7$. (C) Linear plot of resistance vs number of adjacent or separated labeled rings for OPI-7 isotopologues. Data in (C) include OPI-7 data from panel (B) and a new data point for 3a,c,e. Purple data points correspond to structures with adjacent labeled rings. The green data point corresponds to a structure where the labeled rings are separated by unlabeled rings as shown in (A). Error bars represent standard errors and the horizontal black dashed line indicates the resistance of the unlabeled OPI-7 wire.

Theoretical Considerations for the Significant CIE in ^{13}C-Labeled OPI Wires. In the incoherent regime where the very large CIE is observed there are two elementary processes that are potentially influenced by ^{13}C labeling: (i) charge hopping from electrode to wire (or from wire to electrode) and (ii) small polaron hopping of the charge along the molecular wire if the carrier is localized over a few monomers (they are both referred to as polaronic effects in the single molecule electronics literature).[46,47] Both processes are thermally activated, and if they are rate-limiting, then their rate is proportional to the measured current, i.e., the microscopic KIE will be proportional to the observed CIE. There are different mechanisms by which the electron transfer rate is influenced by the nuclear mass. The most common origin of isotopic effects in molecular activated processes, including the two discussed here, is the decrease of the zero point energy (ZPE) of the reactant with respect to the transition state (a kinetic effect).[1−4,48,49] For ^{13}C labeling, this quantity cannot exceed $\frac{1}{2}\hbar\omega_0(1-\sqrt{m_{C13}/m_{C12}}) \approx 0.02\hbar\omega_0$, where $\hbar\omega_0 \approx 0.2$ eV is the largest vibrational frequency that could be involved in the reaction coordinate. This effect could increase the barrier for a reaction including a ^{13}C labeled molecule by up to 4 meV, which would result in reaction rates slower by up to 17%, clearly too far from the observed CIE.

A second important effect that can explain large variations in rate is *nuclear* quantum mechanical tunnelling: The system evolves from reactant to product tunnelling through the potential energy barrier and the relevant masses are those of the nuclei.[50−52] The effect may pertain to both processes of hopping to/from the electrode to the wire or the activated process of polaron hopping along the wire. Some charge transfer theories, e.g., Marcus theory, ignore the nuclear tunneling effect and predict identical rates for isotopically labeled reactants. In theories that include nuclear tunneling effects, from idealized rectangular barrier to explicit calculation of Franck−Condon overlap,[53] the effect of the mass on the rate can be invariably expressed as $k_{nucl\_tunnel} \approx k_0 \exp(-A\sqrt{m_A})$ where m_A is the effective mass of the reaction coordinate (influenced by isotopic labeling), k_0 is the rate prefactor, and A is a parameter collecting all quantum nuclear tunnelling conditions. Clearly, larger masses are associated with slower rates. It follows that the nuclear tunneling rate for the natural abundance carbon isotopologue is larger than for the ^{13}C-labeled molecule by at most a kinetic isotope effect given by $\mathrm{KIE} = \exp(-A(\sqrt{m_{C12}} - \sqrt{m_{C13}}))$. However, by expressing A in terms of KIE we find that the rate must be $k_{nucl\_tunnel} = k_0 \mathrm{KIE}^{-1/\sqrt{m_{C13}/m_{C12}}-1} \approx k_0 \mathrm{KIE}^{-24.5}$, i.e., implausibly slow for any reasonable value of the k_0 prefactor, for the value of KIE ∼ 5 observed in the present experiments.

Isotope effects can also influence equilibrium constants and therefore modify the overall kinetics by modulating the free energy of the reaction intermediates.[54−60] Unlike the kinetic effect on the ZPE, this thermodynamic isotope effect does not have an upper bound as it may involve additively many modes and large changes of vibrational frequencies, e.g. in the case of bond breaking. For the system under study, a strong effect can be seen if the charged wire has a very different ZPE than the neutral one and therefore the energy of injecting a charge in the wire would be different for different isotopic labeling. This was an intriguing possibility considering the distorted nature of the OPI in the ground state that may lead to a different

https://doi.org/10.1021/acsnano.3c11327
ACS Nano 2024, 18, 7444−7454

geometry in the charged state.[28,45] Quantum chemical calculations reported in Tables S4−S8 do not however support this hypothesis: The carrier is delocalized across the wire regardless of its length, but its ZPE-corrected energy is not appreciably influenced by isotopic mass. It should be noted that we did not explore the possibility of reversible bond breaking upon reduction or oxidation of the wire.

There are a few accounts of large isotope effects for $^{13}C/^{12}C$ substitution that are attributed to the coupling between nuclear and electronic spin states via the magnetic isotopic effect.[61−64] This effect is seen in reactions involving triplet states, but our quantum chemical calculations (see Table S9) rule out the energetic proximity of triplets state in the OPI wires. A surprising and unexplained effect of ^{13}C substitution was also reported for transport in carbon nanotubes[65] suggesting that there may be additional mechanisms that enhance the coupling of electrons and ^{13}C nuclei that require further investigation. Further insights into the mechanism are derived by the additional experiments below.

Observation That the ^{13}C CIE Is Structurally Sensitive. Though the cause of the ^{13}C CIE in OPI wires is still an open question, we have proceeded to explore the effect, and in particular we are interested in whether the CIE is sensitive to selective labeling of only certain phenylene rings in the molecules. Therefore, we prepared and measured 6 different structural isotopologues of **OPI-7** evident in Figure 5A and Figures S18−S20. We employ a two-component naming scheme for these isotopologues where we use a number to indicate the number of labeled rings and a letter, or multiple letters, to denote which of the 5 internal rings of the **OPI-7** wires are labeled, as indicated in the figure. The semilog plot in Figure 5B shows that indeed the ^{13}C CIE is sensitive to the number of labeled rings in **OPI-7** (purple points) and all CIE values are summarized in Table 2. Isotopologue **1a** of **OPI-7**, with one labeled ring, does not have a resistance that is distinguishable from the native isotopologue. However, labeling two rings, corresponding to isotopologue **2a,b** for instance, does result in a resistance value that is measurably larger. Likewise labeling 3 rings (**3a,b,c**) and 4 rings (**4a,b,c,d**) results in step increases in the resistance. Also shown in Figure 5B are points for the "fully labeled" **OPI-7** already discussed in Figure 3 (in which 5 of 7 rings are labeled) and the labeled versions of **OPI-8**, **-9**, and **-10**. One can see there is a steady, seemingly exponential, increase in the low bias resistance with the number of labeled rings.

Table 2. Summary of Conductance Isotope Effect (CIE) for Isotopologues of OPI-7[a]

	Structural Isotopomer	Conductance Isotope Effect (CIE)
	1 (*a*)	1.0 ± 0.3
adjacent	**2** (*a*, *b*)	1.8 ± 0.5
	2 (*d*, *e*)	1.4 ± 0.3
	3 (*a*, *b*, *c*)	2.0 ± 0.5
	4 (*a*, *b*, *c*, *d*)	3.7 ± 0.8
separated	**2** (*a*, *c*)	2.0 ± 0.5
	2 (*a*, *d*)	0.9 ± 0.2
	2 (*a*, *e*)	1.0 ± 0.2
	3 (*a*, *c*, *e*)	4.8 ± 0.8

[a]CIE = R_{heavy}/R_{light} where R_{heavy} is the low bias (±0.15 V) resistance of the heavy atom isotopologue and R_{light} is the low bias resistance of the natural abundance isotopologue. Uncertainties are standard errors of the mean.

Figure 5C shows more detailed summaries of our **OPI-7** labeling experiment where we have added results for **2d,e** and **3a,c,e**, whose structures are shown in Figure 5A. Comparison of the resistances in Figure 5C for **2a,b** and **2d,e**, which are isotopomers, indicates that within error the resistances are the same, i.e., the position of the two adjacent labeled rings along the **OPI-7** backbone does not seem to matter. However, we can also observe that **3a,c,e**, in which the labeled rings are separated by unlabeled rings, has approximately 2.5 times greater resistance than isotopomer **3a,b,c** in which all the labeled rings are adjacent to each other. This is a fascinating result which seemingly must contain information about the relative localization or delocalization of charge in the OPI backbone.

Perhaps our most intriguing result is shown in Figure 6. Here we display four isotopomers of **OPI-7** (**2a,b**; **2a,c**; **2a,d**; and **2a,e**) in which the number of unlabeled rings between two labeled rings is systematically increased from 0 to 3. The data are also summarized in Table 2. One can see that there is a stepped decrease in the resistance of nearly 45% between **2a,c** and **2a,d**. It is extremely tempting to attribute this behavior to

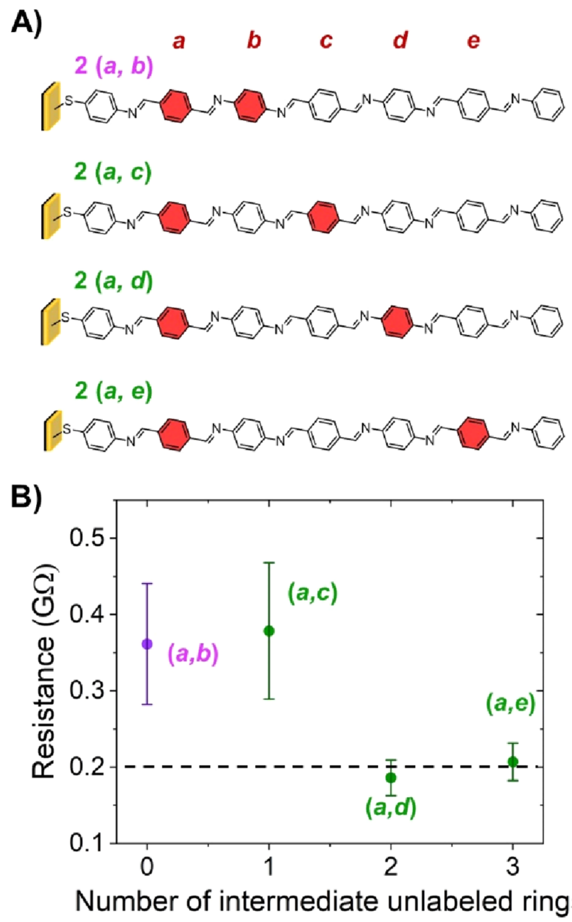

Figure 6. (A) Molecular structures of isotopomers of OPI-7 with two ^{13}C-labeled rings and varying numbers of intermediate unlabeled rings. (B) Plot of resistance vs number of intermediate unlabeled rings for the structures shown in (A). Error bars represent standard errors on the mean, and the horizontal black dashed line indicates the resistance of the unlabeled OPI-7 wire.

https://doi.org/10.1021/acsnano.3c11327
ACS Nano 2024, 18, 7444−7454

a polaron size effect. For example, if we imagine that the polaron in the OPI wires extends over at most three rings at any one time, then in isotopomers **2a,b** and **2a,c** the polaron will encompass 2 labeled rings at one time, whereas for isotopomers **2a,d** and **2a,e** it will only encompass 1 labeled ring. At the current time, though, this hypothesis is at odds with the quantum chemical calculations that suggest that the polaron is completely delocalized across **OPI-7**. In ongoing work, we will seek to examine heavy atom isotope effects in oligomers with alternative architectures, such as aryl alkynes, to check the generality of our observations here on OPI oligomers.

CONCLUSION

In conclusion, we have verified and substantially expanded upon our initial report of conductance isotope effects in OPI wires ranging from 1 to 7 nm in length and connected between metal electrodes. We observe that ^{13}C atom labeling of phenylene rings results in large CIEs, much larger than typical ^{13}C KIEs reported for typical reaction kinetics experiments. Importantly, we also show that the measured CIEs are sensitive to the number and spacing of labeled phenylene rings, i.e., the CIE is structurally sensitive. In principle, such structural sensitivity may be useful in understanding intramolecular conduction mechanisms in molecules and we present initial results in this vein. We have also undertaken a theoretical survey of possible explanations for the ^{13}C CIE. Although we have identified possible explanations that merit further study, a satisfactory description of the experimental results is not currently in place. Nevertheless, the potential importance of this discovery to organic and molecular electronics suggests that further efforts to establish both the generality of the results here, and their fundamental explanation, are warranted.

EXPERIMENTAL SECTION

Materials. Au nuggets (99.999%) were purchased from Mowrey's Inc. (Saint Paul, MN). Cr evaporation rods and evaporation boats were obtained from R. D. Mathis (Long Beach, CA). Si (100) wafers were obtained from WaferNet (San Jose, CA). Contact mode AFM tips (DNP silicon nitride probes) were purchased from Bruker AFM Probes (Camarillo, CA). 4-Aminothiophenol (4-ATP), aminobenzene-$^{13}C_6$ (99 atom % ^{13}C), aminobenzene-D_5 (98 atom % D), benzene-$^{13}C_6$ (99 atom % ^{13}C), benzene-D_6 (99.6 atom % D), aniline (>99.5%), and benzaldehyde (>99%) were purchased from Sigma-Aldrich. Absolute ethanol (200 proof) was purchased from Decon Laboratories (King of Prussia, PA).

***N*-Phenylacetamide-$^{13}C_6$ (2) or *N*-Phenylacetamide-D_5 (2-D).** In a two-necked round-bottomed flask 0.250 g of aniline-$^{13}C_6$ or aniline-D_5 was dissolved in 2 mL of a mixture 1:1 of acetic acid and acetic anhydride and the reaction was heated at 100 °C for 1 h. After the reaction time, the mixture of the reaction mixture was poured onto crushed ice to precipitate the product. The solid was filtered, and the target compound was obtained as a white solid (0.338 g, yield 95% for **2** and 0.332 g, yield 93% for **2-D**). ^{1}H NMR for **2** (400 MHz, $CDCl_3$) δ: 7.69 (m, 1H), 7.50 (m, 1H), 7.40 (br s, 1H), 7.30 (m, 1H), 7.11 (m, 1H), 6.90 (m, 1H), 2.17 (s, 3H). ^{13}C (100 MHz, $CDCl_3$) δ: 168.4, 137.9 (t), 129.0 (t), 124.4 (t), 119.8 (t), 24.6. ^{1}H NMR for **2-D** (400 MHz, $CDCl_3$) δ: 7.23 (br s, 1H), 2.18 (s, 3H). ^{13}C (100 MHz, $CDCl_3$) δ: 168.4, 137.8, 128.7 (t), 123.9 (t), 119.3 (t), 24.8.

***N*-(4-Nitrophenyl)acetamide-$^{13}C_6$ (3) or *N*-(4-Nitrophenyl)-acetamide-D_4 (3-D).** In a one-necked round-bottomed flask 0.300 g of *N*-phenylacetamide-$^{13}C_6$ (**2**) or *N*-phenylacetamide-D_5 (**2-D**) was dissolved in 4 mL of concentrated H_2SO_4, and the solution was cooled down to 0 °C using an ice-acetone bath. Separately, 0.196 g of $NaNO_3$ (1.1 equiv) was dissolved in 2.5 mL of concentrated sulfuric acid, and the solution was cooled to 0 °C and added dropwise to the solution with the starting material during 30 min. Finishing the addition, the reaction was stirred for 30 min between 0 and 5 °C and later poured into crushed ice. The product was filtered and washed with cold water, giving a pale-yellow solid (0.356 g, yield 90% for **3** and 0.370 g, yield 94% for **3-D**). ^{1}H NMR for **3** (400 MHz, DMSO-d_6) δ: 10.55 (s, 1H), 8.42 (m, 1H), 8.01 (m, 2H), 7.58 (m, 1H), 2.12 (s, 3H). ^{13}C (100 MHz, DMSO-d_6) δ: 169.3, 146.0 (t), 142.4 (t), 125.5 (t), 119.0 (t), 24.7. ^{1}H NMR for **3-D** (400 MHz, $CDCl_3$) δ: 10.55 (br s, 1H), 2.12 (s, 3H). ^{13}C (100 MHz, $CDCl_3$) δ: 169.3, 145.3, 141.9, 124.6 (t), 118.1 (t), 24.2.

4-Nitroaniline-$^{13}C_6$ (4) or 4-Nitroaniline-D_4 (4-D). In a one-necked round-bottomed flask, 0.335 g of *N*-(4-nitrophenyl)-acetamide-$^{13}C_6$ (**3**) or *N*-(4-nitrophenyl)acetamide-D_4 (**3-D**) was dissolved in 2.5 mL of hydrochloric acid:water (6:4), and the solution was heated at 80 °C for 1 h. After reaction, the crude mixture was poured onto crushed ice, and the pH was adjusted to 9 using concentrated NH_4OH. The solid was filtered and washed with cold water to give the product as a bright yellow solid (0.254 g, yield 98% for **4** and 0.245 g, yield 95% for **4-D**). ^{1}H NMR for **4** (400 MHz, DMSO-d_6) δ: 7.95 (d, 2H), 6.71 (br s, 2H), 6.58 (d, 2H).^{13}C (100 MHz, DMSO-d_6) δ: 156.1 (t), 136.1 (t), 126.8 (t), 112.8 (t). ^{1}H NMR for **4-D** (400 MHz, DMSO-d_6) δ: 6.70 (br s, 2H). ^{13}C (100 MHz, DMSO-d_6) δ: 155.6, 135.5, 126.0 (t), 112.0 (t).

1,4-Diaminobenzene-$^{13}C_6$ (5) or 1,4-Diaminobenzene-D_4 (5-D). The product was synthesized according to procedures reported in the literature.[66] In a two-necked round-bottomed flask, 0.250 g of 4-nitroaniline-$^{13}C_6$ (**4**) or 4-nitroaniline-D_4 (**4-D**) was dissolved in 3.5 mL of methanol, and 10 mol % of Raney-Ni were added. Later, 0.270 g of $NaBH_4$ (4 equiv) was added at room temperature, and the reaction was heated at 40 °C for 10 min. After the reaction, the solvent was evaporated, and the solids were redissolved in brine. The product was extracted with DCM (3 × 15 mL), and the organic phase was dried using Na_2SO_4. After evaporation, the product was isolated as a pale pink solid (0.178 g, yield 90% for **5** and 0.183 g, yield 93% for **5-D**). ^{1}H NMR for **5** (400 MHz, DMSO-d_6) δ: 6.53 (m, 2H), 6.15 (m, 2H), 4.16 (s, 4H). ^{13}C (100 MHz, DMSO-d_6) δ: 138.8 (m), 115.3 (m). ^{1}H NMR for **5-D** (400 MHz, $CDCl_3$) δ: 6.34, 3.33 (br s, 4H). ^{13}C (100 MHz, $CDCl_3$) δ: 138.6, 116.8 (t).

1,4-Diiodobenzene-$^{13}C_6$ (6) or 1,4-Diiodobenzene-D_4 (6-D). In a two-neck round-bottom flask under nitrogen atmosphere, 1.2 g of $NaIO_4$ (0.7 equiv) and 3.2 g of I_2 (1.8 equiv) were suspended in a mixture of glacial acetic acid (15 mL) and acetic anhydride (10 mL), and the resulting suspension was stirred at 0 °C using an ice/salt bath. Then, 2.5 mL of H_2SO_4 was added dropwise over 1 h. After this time, 1 mL of benzene-$^{13}C_6$ or benzene-D_6 was added, and the reaction mixture was warmed to room temperature and stirred for 4 h. Later, the mixture was poured into an aqueous saturated solution of Na_2SO_3. The precipitate was filtrated and recrystallized from EtOH to give a white solid (3.165 g, yield 90% for **6** and 3.038 g, yield 87% for **6-D**). ^{1}H NMR for **6** (400 MHz, $CDCl_3$) δ: 7.61 (m, 2H), 7.18 (m, 2H). ^{13}C (100 MHz, $CDCl_3$) δ: 139.4 (m), 93.4 (m). ^{1}H NMR for **6-D** (400 MHz, $CDCl_3$) δ: 7.41 (s). ^{13}C NMR for **6-D** (100 MHz, $CDCl_3$) δ: 139.0 (t), 93.2.

Terephthalonitrile-$^{13}C_6$ (7) or Terephthalonitrile-D_4 (7-D). The product was obtained following a procedure reported in the literature.[67,68] In a pressure vessel tube, 1 g of 1,4-diiodobenzene-$^{13}C_6$ (**6**) or 1,4-diiodobenzene-D_4 (**6-D**), 0.581 g of KCN (3 equiv), and 0.566 g of CuI (1 equiv) were suspended in 15 mL of NMP. The mixture was degassed using N_2 for 15 min and heated at 230 °C overnight using an oil bath. After reaction, the mixture was cooled to room temperature and 30 mL of ethyl acetate were added. The resulting mixture was washed with 250 mL of aqueous $FeCl_3$ (10% w/v), 250 mL of $Na_2S_2O_3$ (10% w/v), and 250 mL of brine. Finally, the organic phase was dried with Na_2SO_4, and the solvent was evaporated. The product was purified by silica column chromatography using hexane as the mobile phase to give a white solid (0.296 g, yield 75% for **7** and 0.316 g, yield 80% for **7-D**). ^{1}H NMR for **7** (400 MHz, $CDCl_3$) δ: 8.01 (m, 2H), 7.57 (m, 2H). ^{13}C (100 MHz, $CDCl_3$) δ: 132.9 (m), 117.1 (m), 116.8 (m). ^{1}H NMR for **7-D** (400 MHz,

https://doi.org/10.1021/acsnano.3c11327
ACS Nano 2024, 18, 7444−7454

$CDCl_3$) δ: 7.80. ^{13}C for **7-D** (100 MHz, $CDCl_3$) δ: 132.5 (t), 117.1, 116.6.

Terephthalaldehyde-$^{13}C_6$ (8) or Terephthalaldehyde-D_4 (8-D). In a one-necked round-bottomed flask, 0.200 g of terephthalonitrile-$^{13}C_6$ (**7**) or terephthalonitrile-D_4 (**7-D**) was dissolved in 15 mL of DCM at room temperature, and 4.5 mL of DIBAL-H (3 equiv) was added dropwise. The reaction was stirred for 3 h at room temperature and after that time, 10 mL of aqueous HCl (6 N) was added to the reaction mixture. The resulting emulsion was stirred vigorously for 30 min, and later the product was extracted using DCM (3 × 15 mL). The organic phase was washed with $NaHCO_3$ (5% w/v) and dried with Na_2SO_4, and the solvent was evaporated. The product was isolated as a pale-yellow solid (0.136 g, yield 65% for **8** and 0.157 g, yield 75% for **8-D**). ^1H NMR for **8** (400 MHz, $CDCl_3$) δ: 10.12 (d, 2H), 8.26 (m, 2H), 7.85 (m, 2H). ^{13}C (100 MHz, $CDCl_3$) δ: 191.4, 140.2 (m), 130.2 (m). ^1H NMR for **8-D** (400 MHz, $CDCl_3$) δ: 9.96 (s, 2H), 8.06. ^{13}C (100 MHz, $CDCl_3$) δ: 191.5, 141.2, 130.2

Preparation of Au Substrates and Au-Coated AFM Tips. For RAIRS and high resolution XPS experiments, Au substrates were prepared using a thermal evaporator with a chamber base pressure of ~2×10^{-6} Torr housed in a N_2-filled glovebox (H_2O, O_2 < 0.1 ppm). First, 50 Å of Cr (rate 0.1 Å/s) as an adhesion layer was evaporated on a bare Si wafer, followed by 500 Å of Au (rate 0.6 Å/s). AFM flat metal substrates were prepared by the template-stripping technique in which 5000 Å of Au (10 Å/s) were deposited by e-beam evaporation onto silicon wafers and later silicon chips were glued using Epoxy 377 (EPO-TEK) and cured for 1 h at 120 °C.[22,23,69] Au-coated AFM probes for CP-AFM measurements were prepared in a thermal evaporator depositing 50 Å of Cr followed by 500 Å of Au on DNP silicon nitride probes.

Synthesis of OPI Molecular Wires. Synthesis procedures for molecular wires can be found in Supporting Information in connection with Figures S1−S3.

Reflection−Absorption Infrared Spectroscopy. RAIRS spectra were collected on a Nicolet iS50 spectrometer with a Harrick Seagull accessory for grazing-angle specular reflectance measurements. The infrared beam was incident at 84° from the surface normal and for each sample and background 1500 scans were collected at 2 cm^{-1} resolution after 20 min of purging with dry air.[13,14,19,20]

X-ray Photoelectron Spectroscopy. XPS measurements were performed on a PHI Versa Probe III XPS system (ULVAC-PHI) using a monochromated Al Kα X-ray source (1486.6 eV). The base pressure was 5.0×10^{-8} Pa. During data collection, the pressure was 2.0×10^{-7} Pa. Samples of uncapped wires (**OPI-4P**, **OPI-6P**, and **OPI-8P**) and their isotopologues were mounted on a sample holder using double-sided adhesive tape. The X-ray spot size was 100 μm, and the power was 50 W under 15 kV. The high-resolution spectra of C_{1s}, N_{1s}, and Au_{4f} core-levels were collected using 55 eV pass energy, 0.05 eV/step, and 20 s per step at 45° takeoff angles. The binding energies of all spectra were referenced to the Au $4f_{7/2}$ peak at 84.0 eV. Raw data were treated to remove the background to yield a spectrum with an approximately horizontal background in the Multipak data reduction software. The processed data were fitted in OriginLab software using a Voigt peak function. To show the quality of the fitting in the XPS region for C_{1s}, N_{1s}, and Au_{4f}, the fit parameters are summarized in Tables S1−S3.

Electrical Measurements. For electrical measurements, all of the OPI wires were capped with a terminal aromatic ring using benzaldehyde or aniline depending on the molecular wire. To remove all physisorbed molecules on the surface of the SAMs, all samples were soaked for 1 h in 30 mL of ethanol at 45 °C.

Room Temperature. Current−voltage measurements were carried out using a Conducting Probe AFM (CP-AFM) housed in an Ar-filled glovebox (H_2O, O_2 < 0.1 ppm). For all experiments, the Au-coated tip was brought into contact with the samples under ~1 nN of applied compressive load. Voltages were applied to the tip with a Keithley 236 source measure unit. Voltage was swept at the tip, the sample was grounded, and current−voltage characteristics were recorded. All measured $I-V$ traces crossed over from practically linear at low biases (slope corresponds to the junction low bias conductance G) to gradually more nonlinear $I-V$ behavior at higher biases. For the OPI wires reported here, the low bias conductance was calculated from the linear portion of averaged $I-V$ curves (800 $I-V$ curves at different locations in different samples) measured over ±0.15 V. For the OPI wires longer than 4 nm, the current−voltage characteristics over higher bias ranges (±1.5 V) were also collected (250 $I-V$ curves).

Variable Temperature. Variable temperature measurements of current−voltage characteristics for **OPI-7** and ^{13}C-labeled **OPI-7** were performed with a Molecular Imaging PicoScan using a heating stage in the range from 23 °C (296 K) to 73 °C (346 K). $I-V$ traces were recorded in the range of ±0.15 V, under N_2 flow and <5% relative humidity. In all cases, Au coated tips were brought into contact with samples under ~1 nN load and the temperature was allowed to equilibrate for 10 min before collecting the current−voltage characteristics.

ASSOCIATED CONTENT

Supporting Information

The Supporting Information is available free of charge at https://pubs.acs.org/doi/10.1021/acsnano.3c11327.

> Synthetic procedures, chemical structures of OPI wires, reflection−absorption infrared spectra (RAIR), X-ray photoelectron spectroscopy spectra (XPS), theoretical considerations, $I-V$ characteristics of all OPI wires at low (±0.15 V) and high (±1.5 V) bias and NMR spectra (PDF)

AUTHOR INFORMATION

Corresponding Author

C. Daniel Frisbie − *Department of Chemical Engineering and Materials Science, University of Minnesota, Minneapolis, Minnesota 55455, United States;* orcid.org/0000-0002-4735-2228; Email: frisbie@umn.edu

Authors

Abraham Colin-Molina − *Department of Chemical Engineering and Materials Science, University of Minnesota, Minneapolis, Minnesota 55455, United States;* orcid.org/0000-0002-2425-4254

Tahereh Nematiaram − *Department of Pure and Applied Chemistry, University of Strathclyde, Glasgow G11XL, United Kingdom*

Andy Man Hong Cheung − *Department of Chemical Engineering and Materials Science, University of Minnesota, Minneapolis, Minnesota 55455, United States*

Alessandro Troisi − *Department of Chemistry, University of Liverpool, Liverpool L697ZD, United Kingdom;* orcid.org/0000-0002-5447-5648

Complete contact information is available at: https://pubs.acs.org/10.1021/acsnano.3c11327

Author Contributions

A.C.M. conducted the experiments including material preparation, all measurements, and experimental data analysis, and wrote the first draft. A.M.H.C. carried out a control experiment and analyzed the data. T.N. and A.T. performed the theoretical and computational analysis and contributed to writing. C.D.F. designed and supervised the research, analyzed the data, and cowrote the paper with input from all the authors.

Notes

The authors declare no competing financial interest.

ACKNOWLEDGMENTS

The authors acknowledge the financial support of the U.S. National Science Foundation (NSF) through grants CHE-2003199 and CHE-2304763. Parts of this work were carried out in the Characterization Facility, University of Minnesota, which receives partial support from the NSF through the MRSEC (Award Number DMR-2011401) and the NNCI (Award Number ECCS-2025124) programs. A.T. thanks the European Research Council (Grant No. 101020369) for financial support.

REFERENCES

(1) Wiberg, K. B. The Deuterium Isotope Effect. *Chem. Rev.* **1955**, *55* (4), 713−743.

(2) Westheimer, F. H. The Magnitude of the Primary Kinetic Isotope Effect for Compounds of Hydrogen and Deuterium. *Chem. Rev.* **1961**, *61* (3), 265−273.

(3) Gomez-Gallego, M.; Sierra, M. A. Kinetic Isotope Effects in the Study of Organometallic Reaction Mechanisms. *Chem. Rev.* **2011**, *111*, 4857−4963.

(4) Simmons, E. M.; Hartwig, J. F. On the interpretation of Deuterium Kinetic Isotope Effects in C-H Bond functionalizations by Transition Metal Complexes. *Angew. Chem., Int. Ed.* **2012**, *51*, 3066−3072.

(5) Dale, H. J. A.; Leach, A. G.; Lloyd-Jones, G. C. Heavy-Atom Kinetic Isotope Effects: Primary Interest or Zero Point? *J. Am. Chem. Soc.* **2021**, *143*, 21079−21099.

(6) Paneth, P. Relative Kinetic Isotope Effects of Heavy Atoms. *J. Chem. Phys.* **1985**, *82*, 3705−3706.

(7) Wambua, V.; Hirschi, J. S.; Vetticatt, M. J. Rapid Evaluation of the Mechanism of Buchwald−Hartwig Amination and Aldol Reactions Using Intramolecular ^{13}C Kinetic Isotope Effects. *ACS Catal.* **2021**, *11*, 60−67.

(8) Iannone, R.; Koppmann, R.; Rudolph, J. $^{12}C/^{13}C$ kinetic isotope effects of the gas-phase reactions of isoprene, methacrolein, and methyl vinyl ketone with OH radicals. *Atmos. Environ.* **2009**, *43*, 3103−3110.

(9) Schneider, T. W.; Hren, M.; Ertem, M. Z.; Angeles-Boza, A. M. $[Ru^{II}(tpy)(bpy)Cl]^+$-catalyzed reduction of carbon dioxide. Mechanistic insights by carbon-13 kinetic isotope effect. *Chem. Commun.* **2018**, *54*, 8518−8521.

(10) Schneider, T. W.; Ertem, M. Z.; Muckerman, J. T.; Angeles-Boza, A. M. Mechanism of photocatalytic reduction of CO_2 by $Re(bpy)(CO)_3Cl$ from differences in carbon isotope discrimination. *ACS Catal.* **2016**, *6* (8), 5473−5481.

(11) Rishavy, M. A.; Cleland, W. W. 13C and 15N Kinetic Isotope Effects on the Reaction of Aspartate Aminotransferase and the Tyrosine-225 to Phenylalanine Mutant. *Biochemistry* **2000**, *39* (25), 7546−7551.

(12) Sra, A. K.; Hu, Y.; Martin, G. E.; Snow, D. D.; Ribbe, M. W.; Kohen, A. Competitive 15N Kinetic Isotope Effects of Nitrogenase-Catalyzed Dinitrogen Reduction. *J. Am. Chem. Soc.* **2004**, *126* (40), 12768−12769.

(13) Van Nguyen, Q.; Frisbie, C. D. Hopping Conductance in Molecular Wires Exhibits a Large Heavy-Atom Kinetic Isotope Effect. *J. Am. Chem. Soc.* **2021**, *143*, 2638−2643.

(14) Ho Choi, S.; Kim, B. S.; Frisbie, C. D. Electrical resistance of long conjugated molecular wires. *Science* **2008**, *320*, 1482.

(15) Ishida, T.; Mizutani, W.; Liang, T.-T.; Azehara, H.; Miyake, K.; Sasaki, S.; Tokumoto, H. Conductive Probe AFM Measurements of conjugated Molecular Wires. *Ann. N.Y. Acad. Sci.* **2003**, *1006*, 164−186.

(16) Xie, Z.; Baldea, I.; Haugstad, G.; Frisbie, C. D. Mechanical Deformation Distinguished Tunneling Pathways in Molecular Junctions. *J. Am. Chem. Soc.* **2019**, *141*, 497−504.

(17) Mativetsky, J. M.; Palma, M.; Samorì, P. Exploring Electronic Transport in Molecular Junctions by Conducting Atomic Force Microscopy. *Top. Curr. Chem.* **2008**, *285*, 157−202.

(18) Sangeeth, C. S. S.; Demissie, A. T.; Yuan, L.; Wang, T.; Frisbie, C. D.; Nijhuis, C. A. Comparison of DC and AC Transport in 1.5−7.5 nm Oligophenylene Imine Molecular Wires across Two Junction platforms: Eutectic Ga-In versus Conducting Probe Atomic Force Microscope Junctions. *J. Am. Chem. Soc.* **2016**, *138* (23), 7305−7314.

(19) Luo, L.; Choi, S. H.; Frisbie, C. D. Probing Hopping Conduction in Conjugated Molecular Wires connected to metal electrodes. *Chem. Mater.* **2011**, *23* (3), 631−645.

(20) Choi, S. H.; Frisbie, C. D. Enhanced Hopping Conductivity in Low Band Gap Donor-Acceptor Molecular wires up to 20 nm in Length. *J. Am. Chem. Soc.* **2010**, *132* (45), 16191−16201.

(21) Luo, L.; Balhorn, L.; Vlaisavljevich, B.; Ma, D.; Gagliardi, L.; Frisbie, C. D. Hopping Transport and rectifying behavior in Long Donor-Acceptor Molecular Wires. *J. Phys. Chem. C* **2014**, *118* (46), 26485−26497.

(22) Demissie, A. T.; Haugstad, G.; Frisbie, C. D. Growth of thin, Anisotropic, pi-conjugated molecular films by Stepwise "Click" Assembly of molecular building blocks: Characterizing reactions yields, surface coverage, and film thickness versus addition step number. *J. Am. Chem. Soc.* **2015**, *137*, 8819−8828.

(23) Taherinia, D.; Frisbie, C. D. Photoswitchable Hopping Transport in Molecular wires 4 nm in Length. *J. Phys. Chem. C* **2016**, *120*, 6442−6449.

(24) Afshari, M.; Dinari, M.; Farrokhpour, H.; Zamora, F. Imine-Linked Covalent Organic Framework with a Naphthalene Moiety as a Sensitive Phosphate Ion Sensing. *ACS Appl. Mater. Interfaces* **2022**, *14* (19), 22398−22406.

(25) Xie, X.; Baldea, I.; Demissie, A. T.; Smith, C. E.; Wu, Y.; Haugstad, G.; Frisbie, C. D. Exceptionally Small Statistical Variations in the Transport Properties of Metal−Molecule−Metal Junctions Composed of 80 Oligophenylene Dithiol Molecules. *J. Am. Chem. Soc.* **2017**, *139*, 5696−5699.

(26) Zhang, Y.; Qiu, X.; Gordiichuk, P.; Soni, S.; Krijger, T. L.; Herrmann, A.; Chiechi, R. C. Mechanically and Electrically Robust Self-Assembled Monolayers for Large-Area Tunneling Junctions. *J. Phys. Chem. C* **2017**, *121*, 14920−14928.

(27) Zhang, Y.; Soni, S.; Krijger, T. L.; Gordiichuk, P.; Qiu, X.; Ye, G.; Jonkman, H. T.; Herrmann, A.; Zojer, K.; Zojer, E.; Chiechi, R. C. Tunneling Probability Increases with Distance in Junctions Comprising Self-Assembled Monolayers of Oligothiophenes. *J. Am. Chem. Soc.* **2018**, *140* (44), 15048−15055.

(28) Smith, C. E.; Odoh, S. O.; Ghosh, S.; Gagliardi, L.; Cramer, C. J.; Frisbie, C. D. Length-Dependent Nanotransport and Charge Hopping Bottlenecks in Long Thiophene-Containing pi-conjugated Molecular wires. *J. Am. Chem. Soc.* **2015**, *137* (50), 15732−15741.

(29) Luo, L.; Frisbie, C. D. Length-Dependent Conductance of Conjugated Molecular Wires Synthesized by Stepwise "Click" Chemistry. *J. Am. Chem. Soc.* **2010**, *132* (26), 8854−8855.

(30) Baldea, I., Ed. *Molecular Electronics: An Experimental and Theoretical Approach*; Taylor & Francis Group, 2015.

(31) McCreery, R. I. Molecular Electronic Junctions. *Chem. Mater.* **2004**, *16*, 4477−4496.

(32) Liao, K.-C.; Hsu, L. Y.; Bowers, C. M.; Rabitz, H.; Whitesides, G. M. Molecular Series-Tunneling Junctions. *J. Am. Chem. Soc.* **2015**, *137*, 5948−5954.

(33) Lee, H. J.; Cho, S. J.; Kang, H.; He, X.; Yoon, H. J. Achieving Ultra Low, Zero, and Inverted Tunneling Attenuation Coefficients in Molecular Wires and Extended Conjugation. *Small* **2021**, *17*, No. 2005711.

(34) McCreery, R. L.; Bergren, A. J. Progress with Molecular Electronic Junctions: Meeting Experimental Challenges in Design and Fabrication. *Adv. Mater.* **2009**, *21*, 4303−4322.

(35) Choi, S. H.; Risko, C.; Delgado, M. C. R.; Kim, B.; Bredas, J.-L.; Frisbie, C. D. Transition from Tunneling to Hopping Transport in Long, Conjugated Oligo-Imine Wires Connected to Metals. *J. Am. Chem. Soc.* **2010**, *132*, 4358−4368.

https://doi.org/10.1021/acsnano.3c11327
ACS Nano 2024, 18, 7444−7454

(36) Zhang, X.; Datta, A.; Hrovat, D. A.; Borden, W. T. Calculations Predict a Large Inverse H/D Kinetic Isotope Effect on the Rate of Tunneling in the Ring Opening of Cyclopropylcarbinyl Radical. *J. Am. Chem. Soc.* **2009**, *131* (44), 16002−16003.
(37) Petralia, L. S.; Tsikritea, A.; Loreau, J.; Softley, T. P.; Heazlewood, B. R. Strong inverse kinetic isotope effect observed in ammonia charge exchange reactions. *Nat. Commun.* **2020**, *11*, 173.
(38) Churchill, D. G.; Janak, K. E.; Wittenberg, J. S.; Parkin, G. Normal and Inverse Primary Kinetic Deuterium Isotope Effects for C-H Bond Reductive Elimination and Oxidative Addition Reactions of Molybdenocene and Tungstenocene Complexes: Evidence for Benzene sigma-Complex Intermediates. *J. Am. Chem. Soc.* **2003**, *125* (5), 1403−1420.
(39) Tsikritea, A.; Park, K.; Bertier, P.; Loreau, J.; Softley, T. P.; Heazlewood, B. R. Inverse kinetic isotope effects in the charge transfer reactions of ammonia with rare gas ions. *Chem. Sci.* **2021**, *12*, 10005.
(40) Yang, Y.; Agarwal, R. G.; Hutchison, P.; Rizo, R.; Soudackov, A. V.; Lu, X.; Herrero, E.; Feliu, J. M.; Hammes-Schiffer, S.; Mayer, J. M.; Abruña, H. D. Inverse kinetic isotope effects in the oxygen reduction reaction at platinum single crystals. *Nat. Chem.* **2023**, *15*, 271−277.
(41) Li, F.; Basile, V. M.; Rose, M. J. Electron transfer through surface grown, ferrocene-capped oligophenylene molecular wires (5−50 Å) on n-Si(111) Photoelectrodes. *Langmuir* **2015**, *31*, 7712−7716.
(42) Lu, Q.; Liu, K.; Zhang, H.; Du, Z.; Wang, X.; Wang, F. From tunneling to hopping: A comprehensive Investigation of Charge Transport Mechanism in Molecular Junctions Based on Oligo(p-phenylene ethynylene)s. *ACS Nano* **2009**, *3* (12), 3861−3868.
(43) Hines, T.; Diez-Perez, I.; Hihath, J.; Liu, H.; Wang, Z.-S.; Zhao, J.; Zhou, G.; Mullen, K.; Tao, N. Transition from Tunneling to Hopping in Single Molecular Junctions by Measuring Length and Temperature Dependence. *J. Am. Chem. Soc.* **2010**, *132* (33), 11658−11664.
(44) Alami, F. A.; Soni, S.; Borrini, A.; Nijhuis, C. A. Perspective-Temperature Dependencies and Charge Transport Mechanisms in Molecular Tunneling Junctions Induced by Redox-Reactions. *ECS J. Solid State Sci. Technol.* **2022**, *11*, No. 055005.
(45) Taherinia, D.; Smith, C. E.; Ghosh, S.; Odoh, S. O.; Balhorn, L.; Gagliardi, L.; Cramer, C. J.; Frisbie, C. D. Charge Transport in 4 nm Molecular Wires with interrupted Conjugation: Combined Experimental and Computational Evidence for Thermally Assisted Polaron Tunneling. *ACS Nano* **2016**, *10*, 4372−4383.
(46) Galperin, M.; Ratner, M. A.; Nitzan, A. Hysteresis, Switching, and Negative Differential Resistance in Molecular Junctions: A Polaron Model. *Nano Lett.* **2005**, *5* (1), 125−130.
(47) Kubar, T.; Elstner, M.; Popescu, B.; Kleinekathofer, U. Polaron Effects on Charge Transport through Wires: A multiscale Approach. *J. Chem. Theory Comput.* **2017**, *13* (1), 286−296.
(48) Gonzalez-Lafont, A.; Lluch, J. M. Kinetic Isotope Effects in chemical and biochemical reactions: physical basis and theoretical methods of calculation. *WIRES Comput. Mol. Sci.* **2016**, *6*, 584−603.
(49) Kohen, A.; Limbach, H., Eds. *Isotope Effects in Chemistry and Biology*; Taylor & Francis Group, 2006..
(50) Schreiner, P. R.; Reisenauer, H. P.; Ley, D.; Gerbig, D.; Wu, C.-H.; Allen, W. D. Methylhydroxycarbene: Tunneling Control of a Chemical Reaction. *Science* **2011**, *332*, 1300−1303.
(51) Doubleday, C.; Armas, R.; Walker, D.; Cosgriff, C. V.; Greer, E. M. Heavy-Atom Tunneling Calculations in Thirteen Organic Reactions: Tunneling Contributions are Substantial, and Bell's Formula Closely Approximates Multidimensional Tunneling at ≥ 250 K. *Angew. Chem., Int. Ed.* **2017**, *56*, 13099−13102.
(52) Castro, C.; Karney, W. L. Heavy-Atom Tunneling in Organic Reactions. *Angew. Chem., Int. Ed.* **2020**, *59*, 8355−8366.
(53) Barbara, P. F.; Meyer, T. J.; Ratner, M. A. Contemporary Issues in Electron Transfer Research. *J. Phys. Chem.* **1996**, *100* (31), 13148−13168.
(54) Kotaka, M.; Okamoto, M.; Bigeleisen, J. Anomalous mass effects in isotopic exchange equilibria. *J. Am. Chem. Soc.* **1992**, *114* (16), 6436−6445.
(55) Bigeleisen, J.; Mayer, M. G. Calculation of equilibrium constants for isotopic exchange reactions. *J. Chem. Phys.* **1947**, *15*, 261−267.
(56) Urey, H. C. The thermodynamic properties of isotopic substances. *J. Chem. Soc.* **1947**, 562−581.
(57) Weston, R. E. Anomalous or Mass-Independent Isotope Effects. *Chem. Rev.* **1999**, *99* (8), 2115−2136.
(58) De Petris, G.; Troiani, A. Isotope Effects in Isotope-Exchange Reactions: Evidence for a large 12C/13C Kinetic Isotope Effect in the Gas Phase. *J. Phys. Chem. A* **2008**, *112* (12), 2507−2510.
(59) Dauphas, N.; Schauble, E. A. Mass Fractionation Laws, Mass-Independent Effects, and Isotopic Anomalies. *Annu. Rev. Earth Planet. Sci.* **2016**, *44*, 709−783.
(60) Janak, K. E. Isotope-labeling Studies and Kinetic and Equilibrium Isotope Effects in Organometallic Reactions. In *Comprehensive Organometallic Chemistry III*, 3rd ed.; Elsevier Ltd., 2007; pp 541−571.
(61) Turro, N. J.; Kraeutler, B. Magnetic field and magnetic isotope effects in organic photochemical reactions. A novel probe of reaction mechanisms and a method for enrichment of magnetic isotopes. *Acc. Chem. Res.* **1980**, *13* (10), 369−377.
(62) Buchachenko, A. L. Magnetic Isotope Effect: Nuclear spin control of chemical reactions. *J. Phys. Chem. A* **2001**, *105* (44), 9995−10011.
(63) Buchachenko, A. L. Magnetic Isotope Effect. *Theor. Exp. Chem.* **1995**, *31* (3), 118−126.
(64) Tarasov, V. F.; Bagryanskaya, E. G.; Grishin, Y. A.; Sagdeev, R. Z.; Buchachenko, A. L. Radio Induced $^{12}C/^{13}C$ Magnetic Isotope Effect. *Mendeleev Commun.* **1991**, *1* (3), 85−86.
(65) Kuemmeth, F.; Churchill, H. O. H.; Herring, P. K.; Marcus, C. M. Carbon nanotubes for coherent spintronics. *Mater. Today* **2010**, *13* (3), 18−26.
(66) Pogorelic, I.; Filipan-Litvic, M.; Merkas, S.; Ljubic, G.; Cepanec, I.; Litvic, M. Rapid, efficient and selective reduction of aromatic nitrocompounds with sodium borohydride and Raney nickel. *J. Mol. Catal. A Chem.* **2007**, *274*, 202−207.
(67) Thamyongkit, P.; Muresan, A. Z.; Diers, J. R.; Holten, D.; Bocian, D. F.; Lindsey, J. S. Meso-^{13}C-Labeled Porphyrins for studies of Ground-State Hole Transfer in Multiphorphyrin Arrays. *J. Org. Chem.* **2007**, *72*, 5207−5217.
(68) Carr, R. M.; Cable, K. M.; Wells, G. N.; Sutherland, D. R. A convenient method for cyanation of aromatic iodo compounds. *J. Labelled Compd. Radiopharm.* **1994**, *34*, 887−897.
(69) Kim, B.; Choi, S. H.; Zhu, X.-Y.; Frisbie, C. D. Molecular Tunnel Junctions Based on Pi-Conjugated Oligoacene Thiols and Dithiols between Ag, Au, and Pt Contacts: Effect of Surface Linking Group and Metal Work Function. *J. Am. Chem. Soc.* **2011**, *133*, 19864−19877.

https://doi.org/10.1021/acsnano.3c11327
ACS Nano 2024, 18, 7444−7454